



This is a repository copy of *Stator turn fault detection by 2nd harmonic in instantaneous power for a triple redundant fault-tolerant PM drive*.

White Rose Research Online URL for this paper:
<http://eprints.whiterose.ac.uk/126261/>

Version: Accepted Version

Article:

Wang, B., Wang, J., Griffo, A. orcid.org/0000-0001-5642-2921 et al. (1 more author) (2018) Stator turn fault detection by 2nd harmonic in instantaneous power for a triple redundant fault-tolerant PM drive. *IEEE Transactions on Industrial Electronics*, 65 (9). pp. 7279-7289. ISSN 0278-0046

<https://doi.org/10.1109/TIE.2018.2793188>

© 2018 IEEE. Personal use of this material is permitted. Permission from IEEE must be obtained for all other users, including reprinting/ republishing this material for advertising or promotional purposes, creating new collective works for resale or redistribution to servers or lists, or reuse of any copyrighted components of this work in other works. Reproduced in accordance with the publisher's self-archiving policy.

Reuse

Items deposited in White Rose Research Online are protected by copyright, with all rights reserved unless indicated otherwise. They may be downloaded and/or printed for private study, or other acts as permitted by national copyright laws. The publisher or other rights holders may allow further reproduction and re-use of the full text version. This is indicated by the licence information on the White Rose Research Online record for the item.

Takedown

If you consider content in White Rose Research Online to be in breach of UK law, please notify us by emailing eprints@whiterose.ac.uk including the URL of the record and the reason for the withdrawal request.



eprints@whiterose.ac.uk
<https://eprints.whiterose.ac.uk/>

Stator Turn Fault Detection by 2nd Harmonic in Instantaneous Power for a Triple Redundant Fault-tolerant PM Drive

Bo Wang, *Member IEEE*, Jiabin Wang, *Senior Member, IEEE*, Antonio Griffo, *Member IEEE*, Bhaskar Sen, *Member IEEE*

Abstract—Fast and reliable detection of stator faults is of key importance for fail-safe and fault tolerant machine drives in order to immediately trigger appropriate fault mitigation actions. The paper presents a detailed analytical and experimental analysis of the behavior of a closed loop controlled permanent magnet machine drive under inter-turn fault conditions. It is shown that significant 2nd harmonic components in the dq voltages, currents, instantaneous active power (IAP) and reactive power (IRP) are generated during turn fault conditions. The analyses further show that the increase of the 2nd harmonic in IAP and IRP during fault conditions is comparatively higher than that of voltage and current, making them ideal candidates as turn fault indicators. A turn fault detection technique based on 2nd harmonic in IAP and IRP is implemented and demonstrated for a triple redundant, fault tolerant permanent magnet assisted synchronous reluctance machine (PMA SynRM) drive. The effectiveness of the proposed detection technique over the whole operation region is assessed, demonstrating fast and reliable detection over most of the operating region under both motoring and generating mode.

Index Terms—Fault tolerant, turn fault, fault detection, fault mitigation, 2nd harmonic, active power, reactive power.

I. INTRODUCTION

STATOR insulation is subject to progressive degradation due to electrical loading, thermal cycling, winding vibration and environmental contamination [1]. According to the industrial surveys in [2], stator winding failures account for 21%–37% of the total machine failures. Stator winding degradation may lead to inter-turn, phase to phase or phase to ground failure [3]. Among these failure modes, inter-turn fault might be considered as a worst fault case since it usually only involves few turns, resulting in a very low impedance of the short-circuited path. As a result, large fault current is induced, producing excessive heat which further degrades the insulation between the winding and lamination and eventually leading to complete failure [4]. The high turn fault current can also cause irreversible demagnetization of the magnets [5]. Significant effort has been devolved to fault tolerant machine design [6, 7], fault modeling [8], fault detection and mitigation strategies [9] to avoid or at least alleviate the effects of this severe failure.

Accurate and fast turn fault detection is a prerequisite technique for any fault-tolerant system as it enables the application of fault mitigation actions. Reliable fault detection is also of paramount importance in order to avoid false alarms and associated unnecessary downtime.

Stator insulation diagnosis and monitoring have been extensively investigated in literature [10]. Most of the turn fault detection techniques are based on motor current signal analysis (MCSA) due to the noninvasive nature of current sensing based techniques. MCSA techniques rely on stator current spectrum analysis to identify spectral components associated with the fault or degradation [11]. The turn fault current generates a 2nd harmonic disturbance in the synchronous dq axis reference frame [12]. Consequently, 2nd harmonics emerge in the dq axis currents i_{dq} , and voltages u_{dq} , both for mains-fed and closed loop controlled inverter-fed machine drives. Therefore, 2nd harmonics of currents and voltages in synchronous reference frame have been proposed as fault indicator. In [13], Park transform was applied to the currents to extract fault signature, whose ellipticity indicates the fault severity. The method was further extended in [14] by tracking the component at twice of the fundamental frequency. The amplitude of this spectral component is directly related to the degree of asymmetry of the motor windings as a result of a fault. Essentially, these two methods are exploring the 2nd harmonic in i_{dq} as fault signal [15]. In [16, 17], fault detection was realized by comparing the magnitude of the 2nd harmonics in control voltages, demonstrating that the turn fault severity is proportional to the amplitude of 2nd harmonics. Unfortunately, the synchronous reference frame 2nd harmonics exist in healthy conditions due to natural unbalance in a drive system. Hence, they are not only affected by the machine operating conditions, but also by the controller parameters, further complicating the fault detection strategy.

In [18], it was demonstrated that the instantaneous power, defined by the product of the currents and voltages, has definite advantages since it carries more information than current or voltage signals individually. Both the IAP and IRP have been

Manuscript received June 9, 2017; revised November 26, 2017; accepted December 23, 2017.

Copyright (c) 2014 IEEE. Personal use of this material is permitted. However, permission to use this material for any other purposes must be obtained from the IEEE by sending a request to pubs-permissions@ieee.org.

The authors are with the Department of Electronic and Electrical engineering, The University of Sheffield, Sheffield, S1 3JD United Kingdom (e-mail: bowang.ee@hotmail.com; j.b.wang@sheffield.ac.uk; a.griffo@sheffield.ac.uk; bsen.ee@gmail.com).

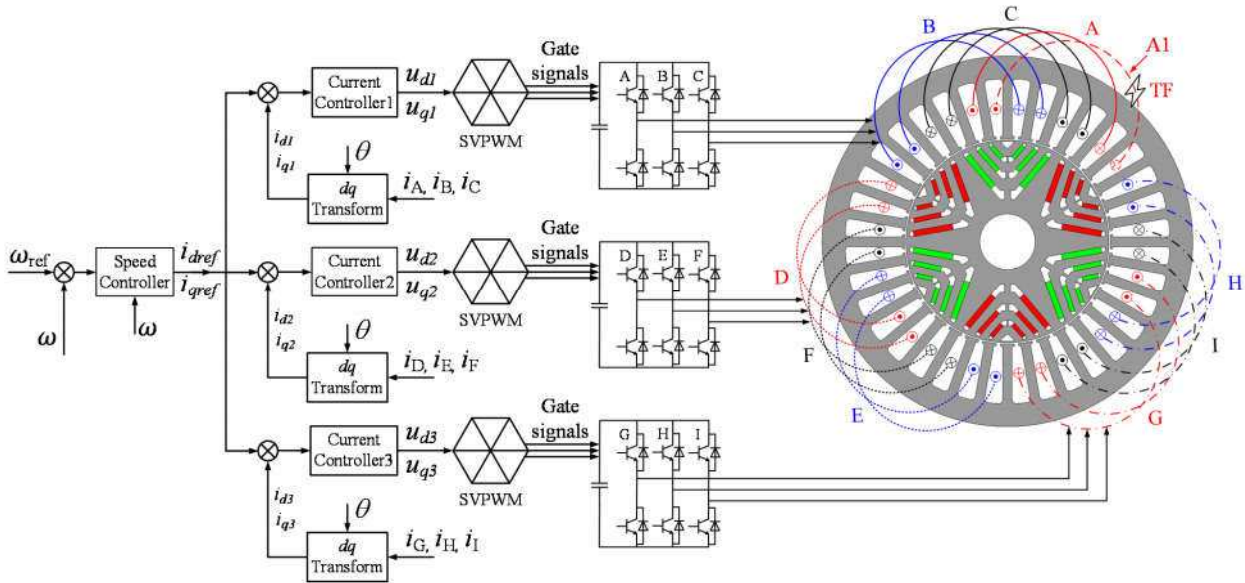


Fig. 1. Triple redundant fault tolerant PMA SynRM drive.

investigated as an indicator to detect various faults for induction machines [19, 20]. It is shown that the stator turn fault results in higher harmonics in IRP than in IAP [21-23]. However, despite some experimental evidence, detailed analytical and physical insight into the causes of these different trends has not been previously reported, nor its applicability to turn fault detection in synchronous PM machine drives assessed and demonstrated.

The main aim of this paper is to develop a simple and reliable turn fault detection technique for closed loop controlled inverter-fed PM drives. Compared to the extraction of the 2nd harmonics of voltages and currents for both dq axes, it is shown that the 2nd harmonic in IAP or IRP provides a stronger fault signature. The proposed fault detection technique is also demonstrated to be fast and relatively computationally inexpensive. Furthermore, theoretical analysis shows that in a closed loop controlled PM machine drive, the turn fault would cause a higher 2nd harmonic in IRP compared to that in IAP when the drive operates in motoring mode, whereas the opposite is true when the drive operates in generating mode. Hence, in motoring mode the 2nd harmonic in IRP is selected as fault indicator while in generating mode the 2nd harmonic in IAP is preferred. The turn fault detection methodology is presented in detail and implemented in a triple redundant, fault tolerant PM drive. Extensive simulation and experimental tests have been performed to confirm the effectiveness of the proposed detection technique over the whole operation region.

II. TURN FAULT MODELLING

The machine under consideration is a 36-slot 6-pole PMA SynRM as shown in Fig. 1. In order to provide enhanced fault tolerance through physical, electrical and thermal isolations, the conventional overlapped windings are divided into three sets of separated 3-phase windings which do not overlap with each other. The electrical isolation is achieved by using three standard 3-phase inverters to drive each 3-phase set. The three

inverter drive modules share the same speed controller which provides the same current references. The current references are tracked by independent current controllers. These segregated windings and independent drives minimize the risk of fault propagation between different 3-phase winding sets and provide redundancy to tolerate various faults [24].

In case of an open-circuit fault in the switches or the windings, the faulty set of windings can be simply deactivated by opening all the switches in that set. If a short circuit failure occurs in the switches or the windings, terminal short circuit can be applied on the faulty set by closing all the bottom or the top switches of the corresponding 3-phase inverter. Since the PM flux in this machine is relatively low, the resultant short circuit currents are lower than the rated. Furthermore, as demonstrated in [24], in case of inter-turn fault, the high fault current can be alleviated by applying a terminal short circuit to the fault set to nullify the external flux. The detection of open circuit, short circuit fault of switches and windings can be relatively easily implemented as discussed in [25-27]. However, the turn fault is potentially more challenging to be detected. This is due to the fact that turn fault typically only involves few turns, resulting in a benign fault signature as seen from machine terminals and consequently a low signal-to-noise ratio. The excessive fault current, however, requires immediate detection and mitigation action. This necessitates a fast and computationally efficient detection within a few tens of milliseconds before developing to a catastrophic failure.

Table I
SPECIFICATIONS OF THE MACHINE

Specification	Symbol	Value
Base speed	n_b	4000rpm
Maximum speed	n_m	19200rpm
Rated power	P_r	35kW
Rated current and gamma angle	I_{rated}	120A(51°)
Nominal DC link voltage	V_{dc}	270V
Turn number of each coil	N	8
Faulty turn number	N_f	1
PM flux linkage	ψ_m	0.025Wb

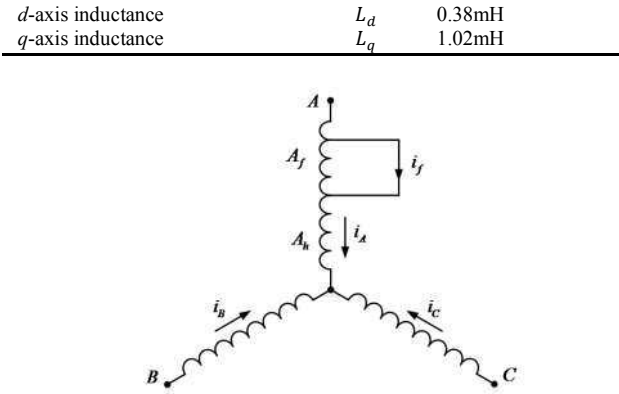


Fig. 2. Schematic circuit for set ABC with turn fault in phase A.

The specifications of the machine are listed in Table I. Without loss of generality, a single turn fault, which has the least fault signature but leads to the highest fault current, is assumed in coil A1 of set ABC as shown in Fig. 1. And the schematic circuit of set ABC windings is shown in Fig. 2. Measurements have shown that a large turn fault current i_f of approximately 8 times of the rated value is induced in the short circuited path. Therefore, this severe fault should be detected immediately and terminal short circuit should be applied on the fault set as a remedial action.

III. FAULT SIGNAL ANALYSIS

In order to develop a reliable turn fault detection method, it is necessary to analyze the fault behavior of the drive under closed loop control and select the fault indicator with the highest signal-to-noise ratio. The 2nd harmonics in the voltage, current and power are of particular interests. These quantities are fundamentally influenced by flux linkages of the windings. In healthy condition and neglecting high order harmonics, the flux linkage of the fault turn is expressed as:

$$\psi_{th} = \varphi \cos(\omega t + \theta_0) \quad (1)$$

where φ , ω and θ_0 represent the magnitude, electrical angular speed and phase angle, respectively.

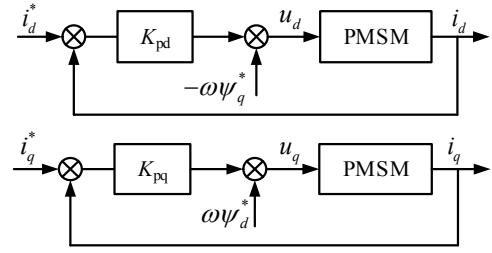
In case of a turn fault, the turn fault current is predominantly reactive and produces flux linkage which opposes the flux linkage in healthy condition. Thus, the flux linkage induced by the fault current can be approximated as:

$$\psi_{tf} = -\varphi_f \cos(\omega t + \theta_0) \quad (2)$$

where φ_f denotes the magnitude of the flux linkage. Transforming this flux linkage to the dq axis yields:

$$\begin{aligned} \Delta\psi_d &= -\frac{1}{3}\varphi_f(\cos\theta_0 + \cos(2\omega t + \theta_0)) \\ \Delta\psi_q &= -\frac{1}{3}\varphi_f(\sin\theta_0 - \sin(2\omega t + \theta_0)) \end{aligned} \quad (3)$$

The 2nd harmonics in the dq flux linkages are seen as disturbances to the current controllers, and consequently cause 2nd harmonics in the voltages and currents. In order to analyze the resultant 2nd harmonic currents and voltages, the current control block diagram is illustrated in Fig. 3. The PI current controller is simplified as a proportional control since the integral control has limited bandwidth and therefore negligible influence at the 2nd harmonic frequency.


 Fig. 3. dq axis current control diagram.

The machine voltage equations can be written as:

$$u_d = \frac{d\psi_d}{dt} - \omega\psi_q, u_q = \frac{d\psi_q}{dt} + \omega\psi_d \quad (4)$$

where the stator resistive drop has been omitted to facilitate the derivation. ψ_d , ψ_q , L_d , L_q denote the d - and q -axis components of flux linkages and inductances, respectively. ψ_d , ψ_q can be expressed as in (5) by accounting for the flux linkage induced by the turn fault current, where DC components of $\Delta\psi_d$, $\Delta\psi_q$ are neglected since their amplitude is relatively small. ψ_m represents the PM flux linkage.

$$\psi_d = \psi_m + L_d i_d - \frac{1}{3}\varphi_f \cos(2\omega t + \theta_0) \quad (5)$$

$$\psi_q = L_q i_q + \frac{1}{3}\varphi_f \sin(2\omega t + \theta_0)$$

The cross coupling compensations, $-\omega\psi_q^*$ and $\omega\psi_d^*$, in the current controller of Fig. 3 are implemented with the estimated values of the dq axis flux linkages as in (6).

$$\psi_d^* = \psi_m + L_d i_d, \psi_q^* = L_q i_q \quad (6)$$

As a result, the voltage equations in (4) by the current feedback control in Fig. 3 can be simplified to:

$$\begin{aligned} -K_{pd} i_d - \frac{\omega}{3}\varphi_f \sin(2\omega t + \theta_0) &= L_d \frac{di_d}{dt} \\ -K_{pq} i_q - \frac{\omega}{3}\varphi_f \cos(2\omega t + \theta_0) &= L_q \frac{di_q}{dt} \end{aligned} \quad (7)$$

The gains K_{pd} and K_{pq} are selected as $\omega_c L_d$ and $\omega_c L_q$, respectively, based on pole-zero cancellation, where ω_c is the current controller bandwidth which is set to 200Hz. By analytically solving (7), the 2nd harmonic currents and voltages in steady state, denoted as i_{d2} , i_{q2} , u_{d2} , u_{q2} , can be derived as:

$$\begin{aligned} i_{d2} &= -\frac{k}{L_d} \sin(2\omega t + \theta_1) \\ i_{q2} &= -\frac{k}{L_q} \cos(2\omega t + \theta_1) \\ u_{d2} &= k(\omega_c \sin(2\omega t + \theta_1) + \omega \cos(2\omega t + \theta_1)) \\ u_{q2} &= k(\omega_c \cos(2\omega t + \theta_1) - \omega \sin(2\omega t + \theta_1)) \end{aligned} \quad (8)$$

$$k = \frac{\omega\varphi_f}{3\sqrt{\omega_c^2 + 4\omega^2}}, \theta_1 = \theta_0 - \tan^{-1} \frac{2\omega}{\omega_c}$$

Defining i_{d0} , i_{q0} as the DC components of i_{dq} , the synchronous currents and voltages can be derived as:

$$\begin{aligned} i_d &= i_{d0} - \frac{k}{L_d} \sin \delta \\ i_q &= i_{q0} - \frac{k}{L_q} \cos \delta \end{aligned} \quad (9)$$

$$u_{d2} = -\omega L_q i_{q0} + k(\omega_c \sin \delta + \omega \cos \delta)$$

$$u_{q2} = \omega \psi_{d0} + k(\omega_c \cos \delta - \omega \sin \delta)$$

$$\psi_{d0} = \psi_m + L_d i_{d0}, \delta = 2\omega t + \theta_1$$

It can be seen that the turn fault induces 2nd harmonics in both currents and voltages. The magnitudes of the 2nd

harmonics are influenced by the current control bandwidth. The IAP and IRP can be calculated as [28]:

$$\begin{aligned} p &= 1.5(u_d i_d + u_q i_q) \\ q &= 1.5(u_q i_d - u_d i_q) \end{aligned} \quad (10)$$

The 2nd harmonics of the active power and reactive power are extracted from (10) and given in (11).

$$\begin{aligned} p_2 &= 1.5k \left(\left(\frac{L_q}{L_d} - 1 \right) \omega i_{q0} + \omega_c i_{d0} \right) \sin \delta + \\ &\quad 1.5k \left(\omega i_{d0} - \frac{\omega \psi_{d0}}{L_q} + \omega_c i_{q0} \right) \cos \delta \\ q_2 &= 1.5k \left(-\frac{\omega \psi_{d0}}{L_d} - \omega i_{d0} - \omega_c i_{q0} \right) \sin \delta + \\ &\quad 1.5k \left(\omega_c i_{d0} - 2\omega i_{q0} \right) \cos \delta \end{aligned} \quad (11)$$

Since the PM flux linkage ψ_m is relatively small and negative i_d is often required for maximum torque per Ampere (MTPA) operation in IPM, ψ_{d0} is quite small compared to the other terms in (11). Hence, the magnitude associated with the *cosine* component of p_2 approximately equals that with the *sine* component of q_2 . Consequently, the magnitude of p_2 depends mainly on its *sine* component while the magnitude of q_2 mostly on its *cosine* component. Comparing the *sine* component of p_2 and the *cosine* component of q_2 , it can be deduced that the magnitude of q_2 will be higher than p_2 when i_{q0} is positive. On the contrary, the magnitude of q_2 will be lower than p_2 with a negative i_{q0} . This means that in motoring mode ($i_{q0} > 0$), the 2nd harmonic in IRP is higher than that of IAP while it is lower than that of IAP in generating mode ($i_{q0} < 0$). It should be noted that the above analysis is based on simplified assumptions and additional causes of the 2nd harmonics in IAP and IRP due to natural machine unbalance and magnetic saturation are not considered. Nonetheless, since the major contributor to the 2nd harmonics is the turn fault, the analysis above demonstrates the relative effects on the proposed fault indicators based on 2nd harmonic characteristics of the IAP and IRP.

In order to understand the 2nd harmonic behavior in the IAP and IRP in turn fault condition over the whole operating region, a turn fault model [29] for the machine under study has been established in MATLAB/SIMULINK. Fig. 4 shows the simulated 2nd harmonics of the IAP and IRP of the faulted 3-phase set in motoring mode and generating mode, respectively. It can be observed that in motoring mode, the induced 2nd harmonic of the IRP in the fault set is higher than that of IAP over the whole torque-speed range while it is lower than that of IAP in generating mode. These results are consistent with the analysis above. Further, the turn fault influence on the 2nd harmonic of IRP in motoring mode and on the 2nd harmonic of IAP in generating mode is more linear across the whole operating region. Therefore, for the purpose of turn fault detection, in motoring mode, the 2nd harmonic in reactive power proves to be a stronger signal whereas in generating mode, the 2nd harmonic of the active power is more preferable. It is also evident that turn fault detection at low speed becomes challenging since the magnitude of the 2nd harmonics diminishes as speed approaches zero.

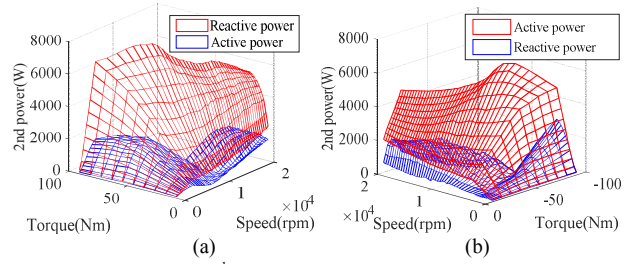


Fig. 4. Comparison of 2nd harmonics in IAP and IRP (a) motoring mode (b) generating mode.

IV. FAULT DETECTION DESIGN

Experimental implementation of the proposed fault detection based on 2nd harmonics in instantaneous power for the closed loop controlled 3x3-phase fault tolerant machine is presented in this section.

It is worth noting that the machine inherent asymmetry and unbalance is inevitable due to manufacturing tolerance, limited accuracies of current sensors [30], and disparity in inverter characteristics. All these factors will contribute to 2nd harmonics in healthy condition. In order to compensate the background 2nd harmonics, lookup tables are produced for each 3-phase set to record the 2nd harmonics in healthy conditions. They are dependent on manufacturing tolerance and disparity in device and material characteristics, and hence differ in each specific machine drive. In most well-manufactured machines, asymmetry will be very small and the resultant 2nd harmonics in IAP and IRP can be obtained automatically during healthy operations. The lookup table covers the whole torque speed range and it is designed as 10x20, 10 points for the torque under each speed, 20 points for the speed in step of 1000rpm.

The 3-phase set with a turn fault due to insulation failure exhibits large 2nd harmonic in the fault indicator. However, the indicator would be significantly lower for the remaining healthy sets. The 2nd harmonics of the healthy set are also simulated and compared with the fault set as shown in Fig. 5 for both operation modes. It can be seen that the induced 2nd harmonics of the fault set are much higher than that of the healthy set. Thus, the 2nd harmonic of each 3-phase set can provide an inherent cross reference to enhance the fault detection. Any harmonics based fault detection might be sensitive to spurious harmonics generated during speed and load changes resulting in false alarms. The application of cross reference between three 3-phase sets can significantly reduce the influence of the speed and load transient on the fault indicators, as such transients will be common to all three sets, while 2nd harmonic is only significantly higher in the fault set, eliminating the risk of false alarms.

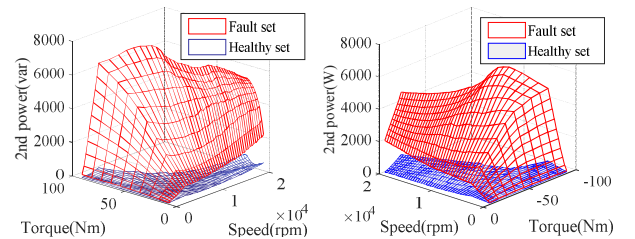


Fig. 5. Comparison 2nd harmonics of faulty and healthy sets (a) IRP in motoring mode (b) IAP in generating mode.

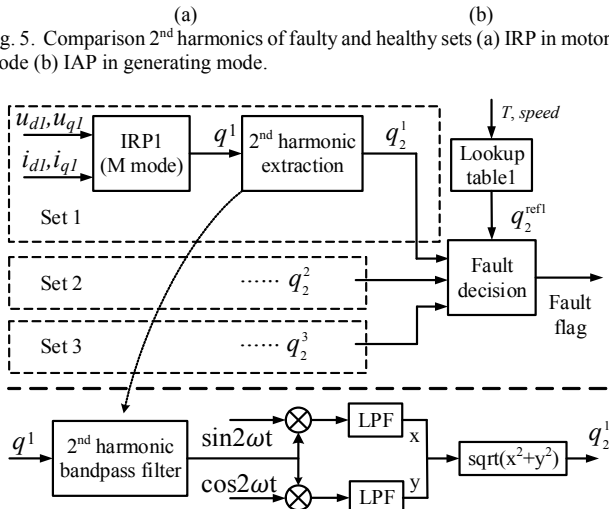


Fig. 6. Fault detection diagram in motoring mode.

A block diagram illustrating the turn fault detection method for motoring mode is shown in Fig. 6. First, the reactive power is calculated based on the control voltages and measured currents using (10). Then the amplitude of the 2nd harmonic is extracted by the filter as shown in the bottom of Fig. 6. Lookup tables provide the reference 2nd harmonic in healthy conditions. Finally, the fault indicators are processed by a fault decision block. The fault flag is triggered if:

$$q_2^1 > 2q_2^{ref1} \text{ AND } q_2^1 > 1.5\max(q_2^2, q_2^3) \quad (12)$$

where q_2^1, q_2^2 and q_2^3 denote the 2nd harmonic in IRP of the ABC, DEF and GHI sets, respectively, and q_2^{ref1} denotes the reference 2nd harmonic of set ABC in healthy condition. The first inequality is verified if the 2nd harmonic is two times higher than its reference in healthy condition while the second inequality indicates that it is also 1.5 times higher than that of the other two sets. The coefficients in the two inequalities can be tuned to maximize detection sensitivity whereas eliminating any false alarm. By means of lookup table and cross reference, the influences of machine unbalance and transients are compensated, ensuring the reliable and accurate detection. The same detection mechanism is also implemented in sets DEF and GHI. The detection in generating mode has been implemented similarly with the only difference being that detection is based on the 2nd harmonic in IAP.

V. EXPERIMENTAL VALIDATION

The proposed turn fault detection technique has been tested on the previously described triple redundant, 9-phase fault tolerant PMA SynRM drive. Fig. 7 shows the test rig where the machine is mounted on a dynamometer via a high precision in-line torque transducer and driven by three independent 3-phase inverters shown in Fig. 8. Each inverter is independently controlled by a digital signal processor (DSP) based current feedback loop. Oil cooling and water cooling have been implemented for the machine and inverter, respectively. The turn fault emulation setup is illustrated in Fig. 9 where a single turn short-circuit in coil B2 of set ABC can be emulated by closing the relay shown in Fig. 9(b). Thick cables are connected

to the fault turn to minimize the additional resistance in the fault path.

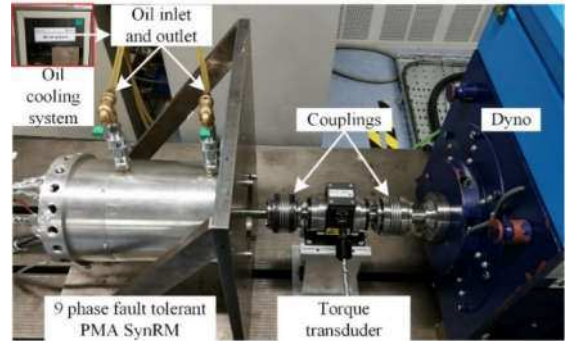


Fig. 7. The 9-phase PMA SynRM drive test rig.

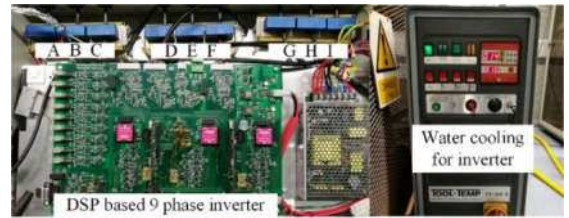


Fig. 8. DSP based closed loop controlled 9 phase inverter.

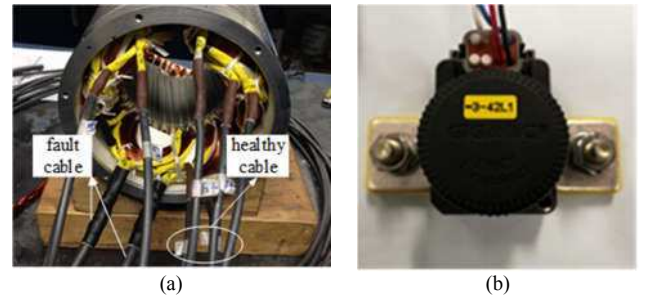


Fig. 9. Turn fault test setup (a) cable leads (b) turn fault relay.

A. Typical Turn Fault Behavior

Since the turn fault current is significantly higher than the rated value, fault occurrence is only tested at low speed to minimize the risk of damage. This does not result in loss of generality as low speed is also the most challenging region for detection. First, the turn fault is injected at 0.06s when the drive operated at 1000rpm with 100A load current and MTPA angle $\gamma = 46^\circ$ in motoring mode. The peak turn fault current shown in Fig. 10 reaches 480A or 4pu. The measured dq currents, i_{dq} , and the resultant dq control voltages, u_{dq} , are shown in Fig. 11 and Fig. 12, where the subscripts 1, 2 and 3 denote the quantities for sets ABC, DEF and GHI, respectively. The IAP and IRP are calculated as shown in Fig. 13. In healthy condition when $t < 0.06$ s, the currents, voltages, IAP and IRP signals are similar for the three 3-phase sets. After the turn fault, the drive continues to operate by the current feedback control. However, noticeable harmonics appear in all signals, and the dominant is clearly the 2nd harmonic. It can be observed that the amplitudes of 2nd harmonic in voltages and currents are relatively small, only a few volts or amperes. In contrast, the 2nd harmonic in IAP and IRP are significantly higher resulting in high signal-to-noise ratio. In agreement with the previously analysis, the 2nd harmonic in IRP is significantly higher than IAP. Therefore, the

2nd harmonic in IRP, q_2 , should be chosen as the fault indicator in motoring mode. The extracted 2nd harmonics in IRP for three 3-phase sets are shown in Fig. 14. As can be seen, in the healthy condition, q_2^1 , q_2^2 and q_2^3 are very small though slightly different due to inherent asymmetries. After the turn fault, q_2^1 increases significantly, whilst q_2^2 and q_2^3 only change slightly in opposite directions. According to the fault judging criteria in (12), the fault detection is accurately triggered.

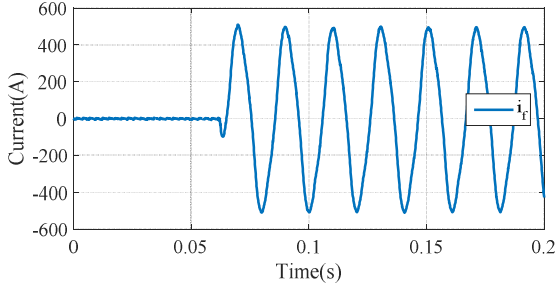


Fig. 10. Turn fault current when the drive operates at 1000rpm and 100A.

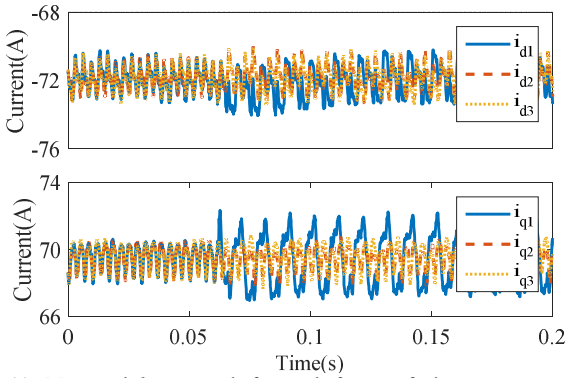


Fig. 11. Measured dq currents before and after turn fault.

Further tests are conducted at 1000rpm with 100A in generating mode. The currents and voltages responses are similar, hence only the IAP and IRP are plotted in Fig. 15. Differently from the motoring mode, now the 2nd harmonic in IAP becomes higher than that of IRP confirming the foregoing analysis. Therefore, in generating mode, the 2nd harmonic of IAP is employed as fault indicator. The processed 2nd harmonics of IAP is shown in Fig. 16. The behavior is similar to that in Fig. 14, hence the turn fault can also be detected reliably.

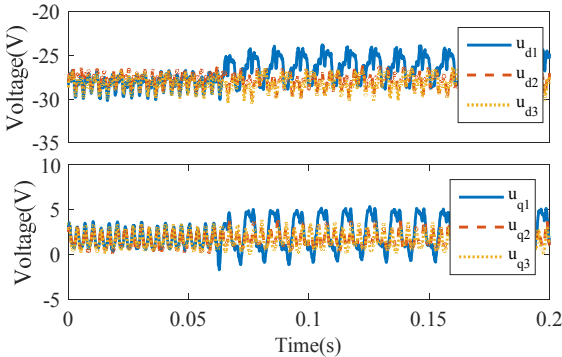


Fig. 12. dq control voltages before and after turn fault.

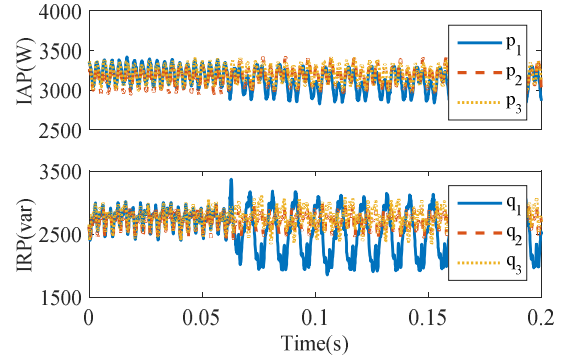


Fig. 13. IAP and IRP before and after turn fault.

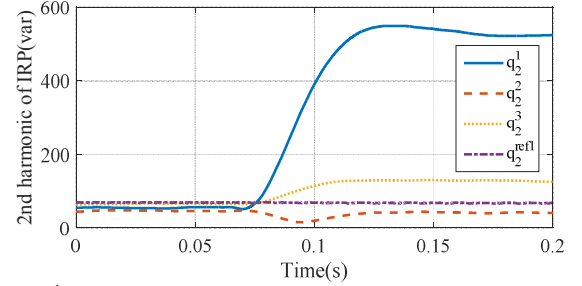


Fig. 14. 2nd harmonics of IRP before and after turn fault.

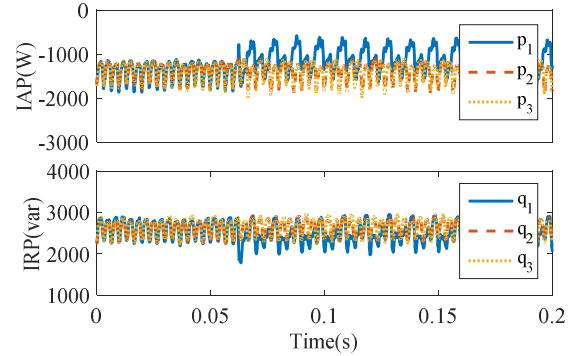


Fig. 15. IAP and IRP before and after turn fault in generating mode.

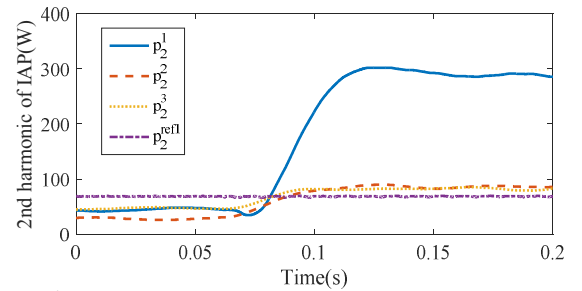


Fig. 16. 2nd harmonics of IAP before and after turn fault in generating mode.

B. Detectability over the Whole Operating Region

An important criterion for fault detection is its detection zone over the torque-speed operating range of the drive. According to Fig. 5, it can be concluded that the most difficult region for the detection is at low speed where the 2nd harmonics in IAP and IRP is quite low. Hence, in addition to the test at 1000 rpm, the proposed detection algorithm is also tested at 500rpm. The ratios of the 2nd harmonic in IRP and IAP, defined as:

$$\text{Ratio} = q_2^1/q_2^{\text{ref}1} \quad \text{motoring mode} \quad (13)$$

$Ratio = p_2^1/p_2^{ref1}$ generating mode
 have been measured in a number of operating conditions in order to evaluate the detectability based on the proposed criteria. The results, shown in Fig. 17, demonstrate that in motoring mode, the ratio is always greater than 2, therefore, the turn fault can be detected in all tested conditions. As expected, the detectability ratio increases with the speed. In generating mode, the ratio under 1000rpm is always higher than 2. However, at 500rpm the ratio drops below 2 when the load current is higher than 90A. This means that turn fault is not detectable in this operating region using a threshold of 2 for the p_2^1/p_2^{ref1} ratio. This effect is caused by a number of reasons. First, at low speed, the turn fault current is intrinsically lower. Furthermore, the resistive drop can no longer be neglected in the fault path and the induced flux is not exactly opposed to the external flux. The fault influence on i_{dq} and u_{dq} is also limited. The voltage drop due to inverter nonlinearities also affects the voltage applied to the machine. In motoring mode, the voltage reference signal is higher than the real voltage due to the inverter voltage drop whilst the opposite is true in generating mode. Hence, the amplitudes of u_{dq} in generating mode are reduced compared to the reference values.

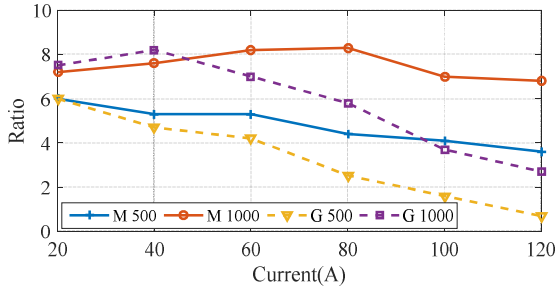


Fig. 17. Detection ratio at 500rpm and 1000rpm in motoring (M500, M1000) and generating (G500, G1000) modes.

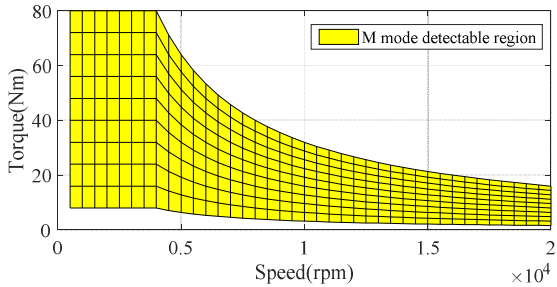


Fig. 18. Detection zone under motoring mode.

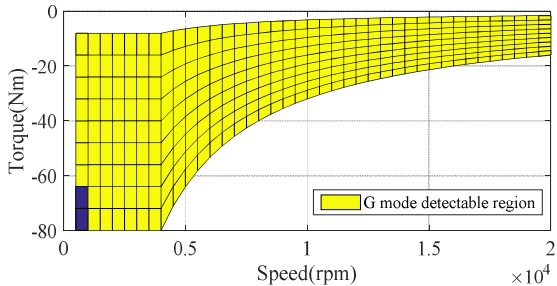


Fig. 19. Detection zone under generating mode.

Based on the analysis above, the detection zones can be expressed as:

$$\begin{aligned} \text{abs}(T) &> 0.1\text{pu} \\ \text{speed} &> 500\text{rpm} \end{aligned} \quad (14)$$

and they are plotted in Fig. 18 and Fig. 19. In motoring mode, all the operating region is detectable whereas in generating mode, only a small region when speed is below 1000rpm and torque is less than -60Nm is not detectable.

C. Detection under Transient Conditions

Fault detection based on harmonics can trigger false alarms during load and speed transients. Robustness of the proposed fault detection is examined for a transient process as shown in Fig. 20. Initially, the machine is loaded with 40A current and MTPA angle $\gamma = 33^\circ$ at 1000rpm, and at $t=0.13\text{s}$ a step change in the current reference from 40A to 60A ($\gamma = 33^\circ$) is applied for all three sets. The filtered responses of the 2nd harmonics are shown in Fig. 21 and they all undergo a transient process during which their magnitudes increase significantly. As can be seen, although the 2nd harmonic amplitude of any 3-phase set is two times higher than the reference value, no false alarm is triggered because the differences in the 2nd harmonics are less than 1.5 times or the second inequality in (12) is not true. A test is also performed when the current step change takes place at 1000 rpm and a single turn fault is injected simultaneously. The 2nd harmonic responses are shown in Fig. 22. In this case, although the 2nd harmonics of all three sets increase during the transient, the 2nd harmonic in the fault set is particularly higher. Thus, the fault can be detected during the transient.

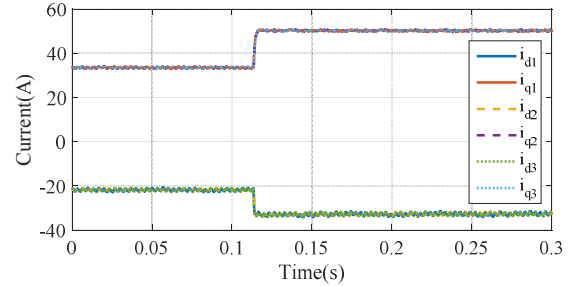


Fig. 20. i_{dq} response in transient.

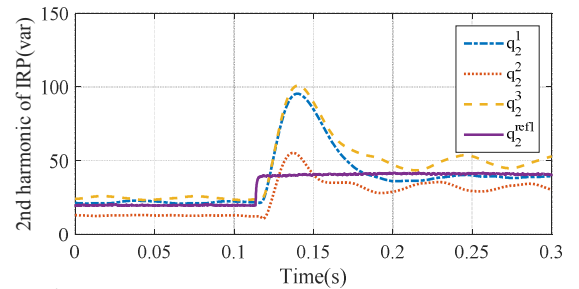


Fig. 21. 2nd harmonic of IRP in transient.

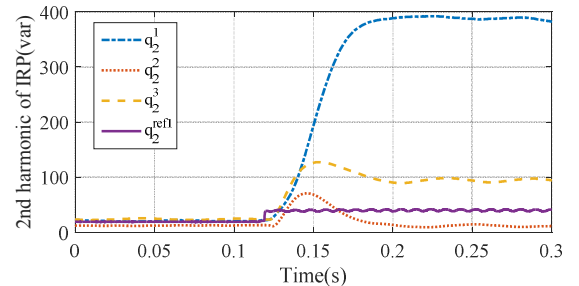


Fig. 22. 2nd harmonic of IRP in transient with turn fault.

To avoid risk of damage in repeated tests with turn fault, simulations are performed in various operating conditions with speed and torque changes. The results show that the fault criterion in (12) yields correct detection in all cases. It follows that by cross-referencing the 2nd harmonics of the three 3-phase sets the proposed fault detection is also effective during transient while false alarm can be avoided. The proposed detection technique is applicable to the conventional 3-phase machines. To ensure no false alarm during transient, however, additional measure is required to discriminate the change in the fault indicator due to speed or load transients in healthy conditions. When the technique is applied to the triple redundant 3x3-phase fault tolerant drive, the false alarm can be eliminated simply by cross reference of the fault indicator of each 3-phase set. Furthermore, the fault detection technique suits very well for the fault tolerant drive and enables fault tolerant operation when a fault is detected and mitigation action is taken.

D. Fault Mitigation Strategy

As previously discussed, the turn fault can be effectively mitigated by applying a terminal short circuit to the faulty set. Experimental validation of the integrated fault tolerant mechanism including the fault detection and mitigation strategy is demonstrated. One turn fault scenario with mitigation is tested at 1000rpm with 60A current under MTPA operation in motoring mode as shown in Fig. 23. Initially, the machine is operating in healthy condition when a single turn fault is triggered by the relay. The fault current increases to 340A which could cause further damage to the machine if no remedial action is applied immediately. This turn fault is detected within one fundamental cycle (less than 15ms) and the mitigation is applied. After the terminal short circuit, the fault current is reduced to 135A which can be thermally sustained indefinitely by the machine. In addition, operation of the other two 3-phase sets are almost not affected, as evident in measured current waveforms of other two sets in Fig. 24, continuing to generate torque. Therefore, the triple 3-phase configuration do not only eliminate the false alarm in transient process, but also enables the fault tolerant operation other than complete failure for the conventional 3-phase machine drive.

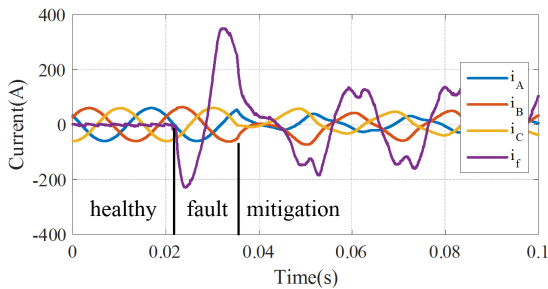


Fig. 23. Integrated fault detection and mitigation behavior.

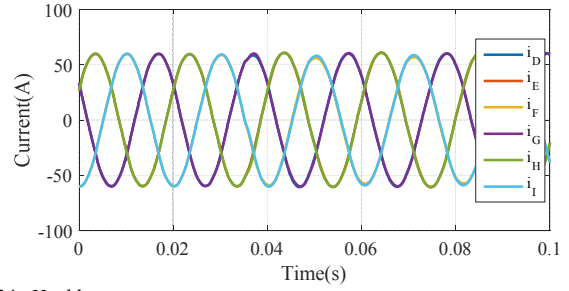


Fig. 24. Healthy sets currents.

VI. DISCUSSIONS

In this section, the factors which may affect the fault detection are discussed by simulation. First, the influence of the current control bandwidth in healthy and fault operations has been analyzed. According to the previous derivation, the 2nd harmonics in the *dq* axis currents, voltages, IAP and IRP are affected by the current controller bandwidth. Therefore, a turn fault is injected at 0.1s when the machine operates in 1000rpm with 60A in motoring mode. The bandwidths of the current controllers are set to 200Hz and 400Hz, respectively. The resultant responses in the *dq* axis currents, voltages and IRP are compared shown in Fig. 25. As can be seen, increase of the control bandwidth from 200Hz to 400Hz does not have significant effect in the healthy operation. In the fault condition, however, the 2nd harmonics in the *dq* currents decrease with the increase of bandwidth while an opposite trend is seen in the voltages. Consequently, the 2nd harmonics in the IRP are almost not affected. By performing fast Fourier transform, the changes in the 2nd harmonics of *dq* axis currents, voltages and IRP are -42%, 10% and -5% respectively. Thus, the IRP is shown insensitive to the current controller bandwidth. The response of the IAP in generating mode is similar and therefore is not presented.

Secondly, the influence of the non-zero impedance in the short circuit path is investigated. External resistance and inductance will reduce fault current and resultant 2nd harmonics. While no additional resistor is inserted in the fault path in testing, the emulated short circuit includes the cable impedance and the relay contact resistance. The external resistance and inductance introduced to the fault that are estimated to be 1.5mΩ and 1μH, respectively. These values are very close to the impedance of the single turn fault. The effect of the turn fault with and without the external impedance is simulated at 1000rpm with 60A load current as shown in Fig. 26. It is found that the turn fault current is reduced by 38% while the 2nd harmonic in the IRP is reduced by 35%. However, the fault can be detected since the resultant 2nd harmonic is much higher than the reference value in the healthy condition. When the external impedance is sufficiently high, the fault cannot be detected, however, the fault current is also much lower and the condition can be thermally contained by the machine.

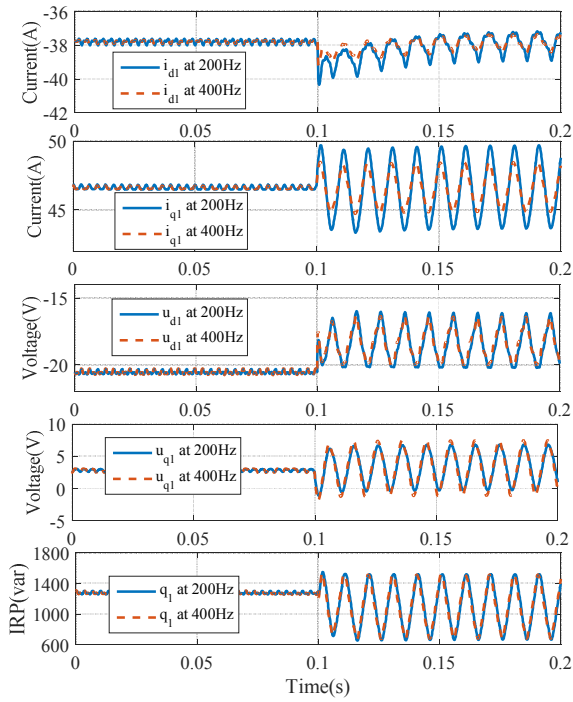


Fig. 25. dq axis currents, voltages and IRP responses with different current controller bandwidths.

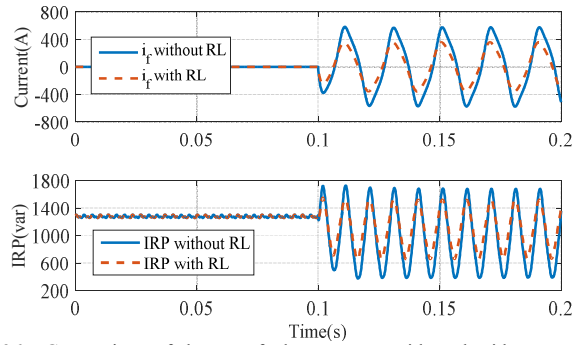


Fig. 26. Comparison of the turn fault responses with and without external impedance.

VII. CONCLUSION

In this paper, a turn fault detection technique has been developed based on the 2nd harmonic in IAP and IRP for a triple redundant, fault tolerant PM machine drive under closed loop control. Analytical derivations, simulations and experiments confirm that the 2nd harmonic in IRP is higher than that of IAP in motoring mode, whilst the opposite is true in generating mode. The analysis demonstrates that the 2nd harmonics in IRP and IAP are suitable indicators for turn fault detection in motoring mode and generating mode, respectively. The proposed detection has been implemented in a triple redundant 9-phase (3x3-phase) machine drive. The effectiveness of the detection technique over the whole operation region has been examined. It is shown that, with the exception of a small low speed region, the proposed technique can detect the turn fault reliably and facilitate the mitigation action to minimize the turn fault current without affecting the healthy sets operation.

VIII. REFERENCES

- [1] A. H. Bonnett and G. C. Soukup, "Cause and analysis of stator and rotor failures in three-phase squirrel-cage induction motors," *Industry Applications, IEEE Transactions on*, vol. 28, pp. 921-937, 1992.
- [2] "Report of Large Motor Reliability Survey of Industrial and Commercial Installations, Part I," *Industry Applications, IEEE Transactions on*, vol. IA-21, pp. 853-864, 1985.
- [3] A. Gandhi, T. Corrigan, and L. Parsa, "Recent Advances in Modeling and Online Detection of Stator Interturn Faults in Electrical Motors," *Industrial Electronics, IEEE Transactions on*, vol. 58, pp. 1564-1575, 2011.
- [4] D. C. Patel and M. C. Chandorkar, "Modeling and Analysis of Stator Interturn Fault Location Effects on Induction Machines," *IEEE Transactions on Industrial Electronics*, vol. 61, pp. 4552-4564, 2014.
- [5] Y. S. Lee, K. T. Kim, and J. Hur, "Finite-Element Analysis of the Demagnetization of IPM-Type BLDC Motor With Stator Turn Fault," *IEEE Transactions on Magnetics*, vol. 50, pp. 889-892, 2014.
- [6] P. Arumugam, "Design Optimization on Conductor Placement in the Slot of Permanent Magnet Machines to Restrict Turn-turn Short-Circuit Fault Current," *IEEE Transactions on Magnetics*, vol. PP, pp. 1-1, 2016.
- [7] J. Dusek, P. Arumugam, C. Brunson, E. K. Amankwah, T. Hamiti, and C. Gerada, "Impact of Slot/Pole Combination on Inter-Turn Short-Circuit Current in Fault-Tolerant Permanent Magnet Machines," *IEEE Transactions on Magnetics*, vol. 52, pp. 1-9, 2016.
- [8] Z. Sun, J. Wang, D. Howe, and G. Jewell, "Analytical Prediction of the Short-Circuit Current in Fault-Tolerant Permanent-Magnet Machines," *Industrial Electronics, IEEE Transactions on*, vol. 55, pp. 4210-4217, 2008.
- [9] J. G. Cintron-Rivera, S. N. Foste, and E. G. Strangas, "Mitigation of Turn-to-Turn Faults in Fault Tolerant Permanent Magnet Synchronous Motors," *IEEE Transactions on Energy Conversion*, vol. 30, pp. 465-475, 2015.
- [10] L. Sang Bin, R. M. Tallam, and T. G. Habetler, "A robust, on-line turn-fault detection technique for induction machines based on monitoring the sequence component impedance matrix," *IEEE Transactions on Power Electronics*, vol. 18, pp. 865-872, 2003.
- [11] S. Nandi, H. A. Toliyat, and X. Li, "Condition monitoring and fault diagnosis of electrical motors-a review," *IEEE Transactions on Energy Conversion*, vol. 20, pp. 719-729, 2005.
- [12] T. Boileau, N. Leboeuf, B. Nahid-Mobarakeh, and F. Meibody-Tabar, "Synchronous Demodulation of Control Voltages for Stator Interturn Fault Detection in PMSM," *IEEE Transactions on Power Electronics*, vol. 28, pp. 5647-5654, 2013.
- [13] A. J. M. Cardoso, S. M. A. Cruz, and D. S. B. Fonseca, "Inter-turn stator winding fault diagnosis in three-phase induction motors, by Park's vector approach," *IEEE Transactions on Energy Conversion*, vol. 14, pp. 595-598, 1999.
- [14] S. M. A. Cruz and A. J. M. Cardoso, "Stator winding fault diagnosis in three-phase synchronous and asynchronous motors, by the extended Park's vector approach," *IEEE Transactions on Industry Applications*, vol. 37, pp. 1227-1233, 2001.
- [15] K. H. Kim, "Simple Online Fault Detecting Scheme for Short-Circuited Turn in a PMSM Through Current Harmonic Monitoring," *IEEE Transactions on Industrial Electronics*, vol. 58, pp. 2565-2568, 2011.
- [16] B. Du, S. Wu, S. Han, and S. Cui, "Interturn Fault Diagnosis Strategy for Interior Permanent-Magnet Synchronous Motor of Electric Vehicles Based on Digital Signal Processor," *IEEE Transactions on Industrial Electronics*, vol. 63, pp. 1694-1706, 2016.
- [17] M. Wolkiewicz, G. Tarcha, x, T. Or, x, K.owska, et al., "Online Stator Interturn Short Circuits Monitoring in the DFOC Induction-Motor Drive," *IEEE Transactions on Industrial Electronics*, vol. 63, pp. 2517-2528, 2016.
- [18] S. F. Legowski, A. H. M. S. Ula, and A. M. Trzynadlowski, "Instantaneous power as a medium for the signature analysis of induction motors," *IEEE Transactions on Industry Applications*, vol. 32, pp. 904-909, 1996.
- [19] M. Drif and A. J. M. Cardoso, "Airgap Eccentricity Fault Diagnosis, in Three-Phase Induction Motors, by the Instantaneous Power Signature Analysis," in *Power Electronics, Machines and Drives, 2006. The 3rd IET International Conference on*, 2006, pp. 349-353.
- [20] M. B. Abadi, S. M. A. Cruz, and A. P. Gon, "Detection of stator and rotor faults in a DFIG based on the stator reactive power analysis," in *IECON 2014 - 40th Annual Conference of the IEEE Industrial Electronics Society*, 2014, pp. 2037-2043.
- [21] M. Drif and A. J. M. Cardoso, "Stator Fault Diagnostics in Squirrel Cage Three-Phase Induction Motor Drives Using the Instantaneous Active and Reactive Power Analyses," *IEEE Transactions on Industrial Informatics*, vol. 10, pp. 1348-1360, 2014.

- [22] M. Drif and A. J. M. Cardoso, "The Use of the Instantaneous-Reactive-Power Signature Analysis for Rotor-Cage-Fault Diagnostics in Three-Phase Induction Motors," *IEEE Transactions on Industrial Electronics*, vol. 56, pp. 4606-4614, 2009.
- [23] M. Drif and A. J. M. Cardoso, "Discriminating the Simultaneous Occurrence of Three-Phase Induction Motor Rotor Faults and Mechanical Load Oscillations by the Instantaneous Active and Reactive Power Media Signature Analyses," *IEEE Transactions on Industrial Electronics*, vol. 59, pp. 1630-1639, 2012.
- [24] B. Wang, J. Wang, and A. Griffo, "A Fault Tolerant Machine Drive Based on Permanent Magnet Assisted Synchronous Reluctance Machine " in *Energy Conversion Congress and Exposition (ECCE), 2016 IEEE*, 2016.
- [25] M. Trabelsi, N. Nguyen, and E. Semail, "Real-Time Switches Fault Diagnosis Based on Typical Operating Characteristics of Five-Phase Permanent Magnetic Synchronous Machines," *IEEE Transactions on Industrial Electronics*, vol. PP, pp. 1-1, 2016.
- [26] Q. T. An, L. Z. Sun, K. Zhao, and L. Sun, "Switching Function Model-Based Fast-Diagnostic Method of Open-Switch Faults in Inverters Without Sensors," *IEEE Transactions on Power Electronics*, vol. 26, pp. 119-126, 2011.
- [27] J. Zhu, N. Ertugrul, and W. L. Soong, "Detection and Remediation of Switch Faults on a Fault Tolerant Permanent Magnet Motor Drive with Redundancy," in *2007 2nd IEEE Conference on Industrial Electronics and Applications*, 2007, pp. 96-101.
- [28] H. Akagi, Y. Kanazawa, and A. Nabae, "Instantaneous Reactive Power Compensators Comprising Switching Devices without Energy Storage Components," *IEEE Transactions on Industry Applications*, vol. IA-20, pp. 625-630, 1984.
- [29] B. Sen, J. Wang, and P. Lazari, "A detailed transient model of Interior Permanent Magnet motor accounting for saturation under stator turn fault," in *Energy Conversion Congress and Exposition (ECCE), 2013 IEEE*, 2013, pp. 3548-3555.
- [30] C. Dae-Woong and S. Seung-Ki, "Analysis and compensation of current measurement error in vector-controlled AC motor drives," *IEEE Transactions on Industry Applications*, vol. 34, pp. 340-345, 1998.



Antonio Griffo (M'13) received the M.Sc. degree in electronic engineering and the Ph.D. degree in electrical engineering from the University of Napoli "Federico II," Naples, Italy, in 2003 and 2007, respectively. From 2007 to 2013, he was a Research Associate with the University of Sheffield, Sheffield, U.K., and the University of Bristol, Bristol, U.K. He is currently a Lecturer with the Department of Electronic and Electrical Engineering, University of Sheffield. His research interests include modeling, control and condition monitoring of electric power systems, power electronics converters, and electrical motor drives, for renewable energy, automotive and aerospace applications.



Bhaskar Sen (M'17) received the B.E. degree from the Delhi College of Engineering, Delhi, India, in 2003, the M.Tech. degree from the Indian Institute of Technology, Kanpur, India, in 2006, both in electrical engineering, and the Ph.D. degree in electrical and electronic engineering from The University of Sheffield, Sheffield, U.K., in 2015. From 2006 to 2011, he was a Research Engineer with GE Global Research, Bangalore, India. From 2015 to 2017, he was a Research Associate at The University of Sheffield. His research interests include electrical machine fault modeling, machine fault detection, and fault-tolerant drives.



Bo Wang (M'17) received the B.Eng. and M.Sc. degrees in electrical engineering from Nanjing University of Aeronautics and Astronautics, Nanjing, China, in 2009 and 2012, respectively. Since 2014, he has been working toward the Ph.D. degree at the Department of Electronic and Electrical Engineering, University of Sheffield, Sheffield, U.K.

From 2012 to 2014, he served as a senior engineer in the Delta Electronics Co. Ltd. Currently, he is working as a research associate at the Department of Electronic and Electrical

Engineering, University of Sheffield. His research interests include the permanent magnet machine drives, electric traction and fault tolerant systems.



Jiabin Wang (SM'03) received the B.Eng. and M.Eng. degrees from Jiangsu University, Zhenjiang, China, in 1982 and 1986, respectively, and the Ph.D. degree from the University of East London, London, U.K., in 1996, all in electrical and electronic engineering.

Currently, he is a Professor in Electrical Engineering at the University of Sheffield, Sheffield, U.K. From 1986 to 1991, he was with the Department of Electrical Engineering at Jiangsu University, where he was appointed a Lecturer in 1987 and an Associated Professor in 1990. He was a Postdoctoral Research Associate at the University of Sheffield, Sheffield, U.K., from 1996 to 1997, and a Senior Lecturer at the University of East London from 1998 to 2001. His research interests range from motion control and electromechanical energy conversion to electric drives for applications in automotive, renewable energy, household appliances and aerospace sectors.

He is a fellow of the IET and a senior member of IEEE.